Sensitivity analysis of generalised eigenproblems and application to wave and finite element models

Cicirello, Alice; Mace, Brian ; Kingan, Michael; Yang, Yi

DOI
10.1016/j.jsv.2020.115345

Publication date
2020

Document Version
Accepted author manuscript

Published in
Journal of Sound and Vibration

Sensitivity analysis of generalised eigenproblems and application to wave and finite element models

Alice Cicirello[1,2*], Brian R Mace[3], Michael J Kingan[3], Yi Yang[3]

1. Department of Engineering Science, Oxford University, Parks Road, Oxford, OX1 3PJ, UK

2. Faculty of Civil Engineering and Geoscience, Delft University of Technology, Stevinweg 1, Delft, 2628CN, Netherlands
a.cicirello@tudelft.nl

3. Acoustics Research Centre, Department of Mechanical Engineering
University of Auckland, Private Bag, Auckland, New Zealand
[b.mace, m.kingan, yi.yang]@auckland.ac.nz

Abstract. The first and second order sensitivity analysis of the eigenvalue problem of generalised, non-symmetric matrices using perturbation theory is developed. These results are then applied to sensitivity analysis of wave propagation in structures modelled using the wave and finite element (WFE) method. Three formulations of the WFE eigenvalue problem are considered: the transfer matrix method, the projection method and Zhong's method. The sensitivities with respect to system parameters of wavenumbers and wave mode shapes are derived. Expressions for the group velocity are presented. Numerical results for a thin beam, a foam core panel and a cross-laminated timber panel are used to demonstrate the proposed approach. It is shown that sensitivities can be calculated at negligible computational cost.

Keywords: generalised eigenproblems; perturbation theory; wave propagation; WFE; Sensitivity analysis.

1. Introduction

The characteristics of wave propagation in structures – wavenumbers, wave mode shapes, group velocity, reflection and transmission coefficients, etc – depend on the material and geometric properties of the medium [1]. Changes (or uncertainties) in these properties result in changes (or uncertainties) in the wave properties. This paper concerns sensitivity analysis relating changes in the physical properties to changes in the wavenumbers and wave mode shapes. A related problem is the estimation of group velocity. The particular emphasis is on complicated structures (e.g. laminates) where analytical solutions are not available and where the wave characteristics are estimated numerically, in this paper using a finite element-based technique. In this wave and finite element (WFE) method [2,3] the dispersion behaviour is found by solving an eigenproblem. Potential applications of the results include: sensitivity analysis, the determination of the most important parameters on which wave behaviour

*Corresponding author

depends and the development of robust designs; model updating and the estimation of physical properties and dispersion behaviour from measurements; uncertainty modelling, relating uncertainties in physical properties to uncertainties in wavenumbers, reflection or transmission coefficients, and hence to uncertainties in vibrational behaviour, response, noise transmission, etc; the estimation of group velocity, which is found from the rate of change of wavenumber with respect to frequency; stability analysis; identification and determination of the cut-off, veering or crossing behaviour of branches of the dispersion curves.

Perturbation theory can be used to evaluate the sensitivity of the eigencharacteristics of a system with respect to changes in a parameter, without requiring the eigenproblem to be solved multiple times. In particular, this approach yields approximate expressions for the eigenvalues and eigenvectors of the perturbed system which are computed via matrix multiplications, reducing the computational cost drastically. When applied to structural dynamics, the system is frequently characterized by symmetric matrices, and therefore much research effort has focused on the analysis of so-called symmetric systems which are characterized by symmetric eigenvalue problems. Solutions for first order perturbations of the eigenproblem for real symmetric matrices with respect to a parameter can be found in [4-7], for example. However, the matrices that result from WFE analysis are asymmetric and often complex [2,3]. As shown also in recent developments on WFE applications to problems on noise transmission [8, 9], periodic structures [10], beams with asymmetric cross-section [11], two-dimensional structures [12, 13], pipes [14] and cylinders [15].

In this paper the first and second order derivatives of the eigensolutions with respect to the system's parameters are derived for generalized, asymmetric eigenproblems. The analysis of real, non-symmetric matrices for the case of weak and strong interaction with equal eigenvalues was considered by Seyranian [5-7]. The problem of distinct eigenvalues was addressed in [5] but did not include results for the second order sensitivity. Recent developments on this topic have been presented in [16]. The eigensolutions derivatives found below are then applied to WFE models, for which the matrices involved are asymmetric and normally complex.

The paper is organised as follows. The generalised eigenproblem and eigensolution sensitivities are presented in section 2. Both first and second order perturbations are developed. Three forms of the WFE eigenvalue problem and their perturbations are discussed in section 3. Estimation of the group velocity is discussed. Section 4 contains numerical examples concerning eigenvalue sensitivities, while section 5 contains the conclusions.

2. The generalised eigenproblem and eigensolution sensitivities

This section presents the sensitivities of the eigenvalues and eigenvectors of the generalised eigenvalue problem. The analysis follows that in [5] with additional expressions for the second order sensitivities being developed below.

2.1 The generalised eigenproblem for fixed system parameters

Let us consider the generalized eigenvalue problem (EP) expressed as

$$\mathbf{B}(\mathbf{p})\mathbf{u} = \lambda \mathbf{C}(\mathbf{p})\mathbf{u}\,, \tag{1}$$

where $\mathbf{B}(\mathbf{p})$ and $\mathbf{C}(\mathbf{p})$ are complex, non-symmetric system matrices of dimensions $m \times m$ (with $\mathbf{C}(\mathbf{p})$ being non-singular) and are functions of n real system parameters in the $n \times 1$ vector $\mathbf{p}$. Here λ and $\mathbf{u}$ are the eigenvalue and right eigenvector. The left EP

$$\mathbf{z}^T\mathbf{B}(\mathbf{p}) = \lambda \mathbf{z}^T\mathbf{C}(\mathbf{p})\,, \tag{2}$$

involves the left eigenvector $\mathbf{z}$. For specific values of the parameters $\mathbf{p} = \mathbf{p}_0$, the two EPs can be written as

$$\mathbf{B}_0\mathbf{u}_0 = \lambda_0\mathbf{C}_0\mathbf{u}_0; \quad \mathbf{z}_0^T\mathbf{B}_0 = \lambda_0\mathbf{z}_0^T\mathbf{C}_0; \tag{3}$$

where $\mathbf{B}_0 = \mathbf{B}(\mathbf{p}_0)$ and $\mathbf{C}_0 = \mathbf{C}(\mathbf{p}_0)$, and $\mathbf{z}_0$ and $\mathbf{u}_0$ are the left and right eigenvectors which are normalised such that

$$\mathbf{z}_0^T\mathbf{C}_0\mathbf{u}_0 = 1. \tag{4}$$

The *j*th and *k*th eigenvectors also satisfy the orthogonality conditions

$$\mathbf{z}_{0,k}^T\mathbf{C}_0\mathbf{u}_{0,j} = \delta_{jk}; \quad \mathbf{z}_{0,k}^T\mathbf{B}_0\mathbf{u}_{0,j} = \lambda_{0,j}\delta_{jk}\,, \tag{5}$$

being δ_{jk} the Kronecker delta (i.e. $\delta_{jj} = 1$ and $\delta_{jk} = 0$ for $j \neq k$). The following derivations will be made for the *j*th eigenvalue and the corresponding eigenvector. For simplifying the notation, the subscript *j* will be omitted in what follows.

2.2 Perturbation of the eigenproblem

Consider a perturbation of order ε of the system parameters $\mathbf{p}_0$ in an arbitrary vector of variation $\mathbf{e} = \left(e_1, ..., e_n\right)^T$, such that

$$\mathbf{p} = \mathbf{p}_0 + \varepsilon \mathbf{e}; \qquad \|\mathbf{e}\| = 1. \tag{6}$$

As a result, the system matrices can be expressed as

$$\mathbf{B} = \mathbf{B}_0 + \varepsilon \mathbf{B}_1 + \varepsilon^2 \mathbf{B}_2 + ...; \quad \mathbf{C} = \mathbf{C}_0 + \varepsilon \mathbf{C}_1 + \varepsilon^2 \mathbf{C}_2 + ... \tag{7}$$

where

$$\mathbf{B}_1 = \sum_{r=1,n} \frac{\partial \mathbf{B}}{\partial p_r} e_r; \qquad \mathbf{C}_1 = \sum_{r=1,n} \frac{\partial \mathbf{C}}{\partial p_r} e_r; \tag{8}$$

$$\mathbf{B}_2 = \frac{1}{2} \sum_{r,s=1,n} \frac{\partial^2 \mathbf{B}}{\partial p_r \partial p_s} e_r e_s; \quad \mathbf{C}_2 = \frac{1}{2} \sum_{r,s=1,n} \frac{\partial^2 \mathbf{C}}{\partial p_r \partial p_s} e_r e_s, \tag{9}$$

where all the partial derivatives are evaluated at $\mathbf{p} = \mathbf{p}_0$. Consequently, each eigenvalue and right eigenvectors can be expanded as powers series in ε as

$$\lambda = \lambda_0 + \varepsilon \lambda_1 + \varepsilon^2 \lambda_2 + ...; \quad \mathbf{u} = \mathbf{u}_0 + \varepsilon \mathbf{u}_1 + \varepsilon^2 \mathbf{u}_2 + ... \tag{10}$$

where, in a similar fashion to Eq. (8) and Eq. (9),

$$\lambda_1 = \sum_{r=1,n} \frac{\partial \lambda}{\partial p_r} e_r; \qquad \mathbf{u}_1 = \sum_{r=1,n} \frac{\partial \mathbf{u}}{\partial p_r} e_r; \tag{11}$$

$$\lambda_2 = \frac{1}{2} \sum_{r,s=1,n} \frac{\partial^2 \lambda}{\partial p_r \partial p_s} e_r e_s; \quad \mathbf{u}_2 = \frac{1}{2} \sum_{r,s=1,n} \frac{\partial^2 \mathbf{u}}{\partial p_r \partial p_s} e_r e_s, \tag{12}$$

and where all the partial derivatives are evaluated at $\mathbf{p} = \mathbf{p}_0$.

2.3 First order perturbation of the eigensolution

The first order derivative of the eigenvalue λ_1, assuming that the unperturbed eigenvalues λ_o are distinct, can be obtained by substituting Eqs. (6) and (7) in Eq. (1), using the normality and orthogonality conditions (Eqs. (4) and (5)) and keeping the first order terms, resulting in

$$\frac{\partial \lambda}{\partial p_r} = \mathbf{z}_0^T \left[\mathbf{B}_1 - \lambda_0 \mathbf{C}_1 \right] \mathbf{u}_0 \tag{13}$$

The same result can be obtained by considering the derivative with respect to the parameter p_r of the eigenvalue problem in Eq. (1) [5]. This can be rewritten as

$$\left(\mathbf{B}_0 - \lambda_0 \mathbf{C}_0 \right) \frac{\partial \mathbf{u}}{\partial p_r} = \left(\lambda_0 \frac{\partial \mathbf{C}}{\partial p_r} + \mathbf{C}_0 \frac{\partial \lambda}{\partial p_r} - \frac{\partial \mathbf{B}}{\partial p_r} \right) \mathbf{u}_0 \tag{14}$$

Eq. (14) is a linear algebraic system with unknown derivatives $\partial \lambda / \partial p_r$ and $\partial \mathbf{u} / \partial p_r$. Since the matrix $\left(\mathbf{B}_0 - \lambda_0 \mathbf{C}_0 \right)$ is singular, the solution of Eq. (14) exists if and only if

$$\mathbf{z}_0^T \left(\lambda_0 \frac{\partial \mathbf{C}}{\partial p_r} + \mathbf{C}_0 \frac{\partial \lambda}{\partial p_r} - \frac{\partial \mathbf{B}}{\partial p_r} \right) \mathbf{u}_0 = 0 \tag{15}$$

Pre-multiplying the left and the right hand side of Eq. (14) by $\mathbf{z}_0^T$, and noting the results in Eq. (3), it follows that [5]

$$\frac{\partial \lambda}{\partial p_r} = \frac{\mathbf{z}_0^T \left(\dfrac{\partial \mathbf{B}}{\partial p_r} - \lambda_0 \dfrac{\partial \mathbf{C}}{\partial p_r} \right) \mathbf{u}_0}{\mathbf{z}_0^T \mathbf{C}_0 \mathbf{u}_0} \tag{16}$$

Given the normalization condition in Eq. (4), Eq. (16) reduces to Eq. (13).

As shown in [5], the expression for $\mathbf{u}_1$ is obtained by differentiating Eq. (4) so that

$$\mathbf{z}_0^T \mathbf{C}_0 \frac{\partial \mathbf{u}}{\partial p_r} = 0 \,. \tag{17}$$

Multiplying this equation by the complex conjugate of the left eigenvector $\overline{\mathbf{z}}_0$, and adding this term to the LHS of Eq. (14) [5,17], it follows that [5]

$$\frac{\partial \mathbf{u}}{\partial p_r} = \Gamma_0^{-1} \left(\lambda_1 \mathbf{C}_0 + \lambda_0 \mathbf{C}_1 - \mathbf{B}_1 \right) \mathbf{u}_0 \tag{18}$$

where Γ_0 is a non-singular matrix given by [5]

$$\Gamma_0 = \mathbf{B}_0 - \lambda_0 \mathbf{C}_0 + \overline{\mathbf{z}}_0 \mathbf{z}_0^{\mathrm{T}} \mathbf{C}_0 \tag{19}$$

Eqs. (13) and (18) are first-order perturbations of the eigensolutions for the non-symmetric system of Eq. (1) with matrices of dimensions $m \times m$. These results reduce to those for symmetric eigenproblems for which **B**, **C** are real and symmetric and the left and right eigenvectors are equal.

When there is only a single parameter *p*, Eqs. (13) and (18) reduce to

$$\frac{\partial \lambda}{\partial p} = \mathbf{z}_0^T \left[\mathbf{B}_1 - \lambda_0 \mathbf{C}_1 \right] \mathbf{u}_0; \tag{20}$$

$$\frac{\partial \mathbf{u}}{\partial p} = \left(\mathbf{B}_0 - \lambda_0 \mathbf{C}_0 + \overline{\mathbf{z}}_0 \mathbf{z}_0^{\mathrm{T}} \mathbf{C}_0 \right)^{-1} \left(\lambda_1 \mathbf{C}_0 + \lambda_0 \mathbf{C}_1 - \mathbf{B}_1 \right) \mathbf{u}_0; \tag{21}$$

with

$$\mathbf{B}_1 = \frac{\partial \mathbf{B}}{\partial p}; \quad \mathbf{C}_1 = \frac{\partial \mathbf{C}}{\partial p}. \tag{22}$$

2.4 Second order perturbation of the eigensolution

The second order derivatives of the eigenproperties can be used to investigate local curvature effects, and therefore wave phenomena such as cut-off, veering and locking. The second order derivatives of the eigenvalues can be found by taking the derivatives of the eigenvalue problem in Eq. (1) with respect to the parameters p_r and p_s. This can be written as

$$\begin{aligned} \left(\mathbf{B}_0 - \lambda_0 \mathbf{C}_0 \right) \frac{\partial^2 \mathbf{u}}{\partial p_r \partial p_s} = & \left(\lambda_0 \frac{\partial^2 \mathbf{C}}{\partial p_r \partial p_s} + \mathbf{C}_0 \frac{\partial^2 \lambda}{\partial p_r \partial p_s} - \frac{\partial^2 \mathbf{B}}{\partial p_r \partial p_s} \right) \mathbf{u}_0 + \mathbf{C}_0 \left(\frac{\partial \lambda}{\partial p_r} \frac{\partial \mathbf{u}}{\partial p_s} + \frac{\partial \lambda}{\partial p_s} \frac{\partial \mathbf{u}}{\partial p_r} \right) + \\ & 2 \left(\frac{\partial \lambda}{\partial p_r} \frac{\partial \mathbf{C}}{\partial p_s} + \frac{\partial \lambda}{\partial p_s} \frac{\partial \mathbf{C}}{\partial p_r} \right) \mathbf{u}_0 + \lambda_0 \left(\frac{\partial \mathbf{C}}{\partial p_r} \frac{\partial \mathbf{u}}{\partial p_s} + \frac{\partial \mathbf{C}}{\partial p_s} \frac{\partial \mathbf{u}}{\partial p_r} \right) - \left(\frac{\partial \mathbf{B}}{\partial p_r} \frac{\partial \mathbf{u}}{\partial p_s} + \frac{\partial \mathbf{B}}{\partial p_s} \frac{\partial \mathbf{u}}{\partial p_r} \right) \end{aligned} \tag{23}$$

As for the first order case, since $\left(\mathbf{B}_0 - \lambda_0 \mathbf{C}_0 \right)$ is singular, Eq. (23) has a solution if and only if the terms on the RHS of Eq. (23) premultiplied by $\mathbf{z}_0^T$ equal zero. Moreover, because of Eq. (3), the second order derivative of the eigenvalue is

$$\frac{\partial^2\lambda}{\partial p_r\partial p_s}=\mathbf{z}_0^T\left[\begin{array}{l}\left(\dfrac{\partial^2\mathbf{B}}{\partial p_r\partial p_s}-\lambda_0\dfrac{\partial^2\mathbf{C}}{\partial p_r\partial p_s}\right)\mathbf{u}_0+\left(\dfrac{\partial\mathbf{B}}{\partial p_r}-\lambda_0\dfrac{\partial\mathbf{C}}{\partial p_r}\right)\dfrac{\partial\mathbf{u}}{\partial p_s}\\+\left(\dfrac{\partial\mathbf{B}}{\partial p_s}-\lambda_0\dfrac{\partial\mathbf{C}}{\partial p_s}\right)\dfrac{\partial\mathbf{u}}{\partial p_r}-\mathbf{C}_0\left(\dfrac{\partial\lambda}{\partial p_r}\dfrac{\partial\mathbf{u}}{\partial p_s}+\dfrac{\partial\lambda}{\partial p_s}\dfrac{\partial\mathbf{u}}{\partial p_r}\right)-2\left(\dfrac{\partial\lambda}{\partial p_r}\dfrac{\partial\mathbf{C}}{\partial p_s}+\dfrac{\partial\lambda}{\partial p_s}\dfrac{\partial\mathbf{C}}{\partial p_r}\right)\mathbf{u}_0\end{array}\right]/\left(\mathbf{z}_0^T\mathbf{C}_0\mathbf{u}_0\right)\ .\tag{24}$$

Because of Eq. (4) and (17), and by differentiating Eq. (4) so that

$$\mathbf{z}_0^T\frac{\partial\mathbf{C}}{\partial p_r}\mathbf{u}_0=0\,,\tag{25}$$

Eq. (24) can be now written as

$$\frac{\partial^2\lambda}{\partial p_r\partial p_s}=\mathbf{z}_0^T\left[\left(\frac{\partial^2\mathbf{B}}{\partial p_r\partial p_s}-\lambda_0\frac{\partial^2\mathbf{C}}{\partial p_r\partial p_s}\right)\mathbf{u}_0+\left(\frac{\partial\mathbf{B}}{\partial p_r}-\lambda_0\frac{\partial\mathbf{C}}{\partial p_r}\right)\frac{\partial\mathbf{u}}{\partial p_s}+\left(\frac{\partial\mathbf{B}}{\partial p_s}-\lambda_0\frac{\partial\mathbf{C}}{\partial p_s}\right)\frac{\partial\mathbf{u}}{\partial p_r}\right]\tag{26}$$

The expression for $\mathbf{u}_2$ can be obtained by differentiating Eq. (4) giving

$$\mathbf{z}_0^T\mathbf{C}_0\frac{\partial^2\mathbf{u}}{\partial p_r\partial p_s}=0\,.\tag{27}$$

Multiplying this equation by the complex conjugate left eigenvector $\bar{\mathbf{z}}_0$, and adding this term to the left hand side of Eq. (23), we find that

$$\frac{\partial^2\mathbf{u}}{\partial p_r\partial p_s}=\Gamma_0^{-1}\left[\begin{array}{l}\left(\lambda_0\dfrac{\partial^2\mathbf{C}}{\partial p_r\partial p_s}+\mathbf{C}_0\dfrac{\partial^2\lambda}{\partial p_r\partial p_s}-\dfrac{\partial^2\mathbf{B}}{\partial p_r\partial p_s}\right)\mathbf{u}_0+\mathbf{C}_0\left(\dfrac{\partial\lambda}{\partial p_r}\dfrac{\partial\mathbf{u}}{\partial p_s}+\dfrac{\partial\lambda}{\partial p_s}\dfrac{\partial\mathbf{u}}{\partial p_r}\right)+\\+2\left(\dfrac{\partial\lambda}{\partial p_r}\dfrac{\partial\mathbf{C}}{\partial p_s}+\dfrac{\partial\lambda}{\partial p_s}\dfrac{\partial\mathbf{C}}{\partial p_r}\right)\mathbf{u}_0+\lambda_0\left(\dfrac{\partial\mathbf{C}}{\partial p_r}\dfrac{\partial\mathbf{u}}{\partial p_s}+\dfrac{\partial\mathbf{C}}{\partial p_s}\dfrac{\partial\mathbf{u}}{\partial p_r}\right)-\left(\dfrac{\partial\mathbf{B}}{\partial p_r}\dfrac{\partial\mathbf{u}}{\partial p_s}+\dfrac{\partial\mathbf{B}}{\partial p_s}\dfrac{\partial\mathbf{u}}{\partial p_r}\right)\right]\end{array}\right]\ .\tag{28}$$

When there is only a single variable parameter *p*, Eqs. (26) and (28) reduce to

$$\frac{\partial^2\lambda}{\partial p^2}=\mathbf{z}_0^T\left[2\left(\mathbf{B}_2-\lambda_0\mathbf{C}_2\right)\mathbf{u}_0+2\left(\mathbf{B}_1-\lambda_0\mathbf{C}_1\right)\mathbf{u}_1\right];\tag{29}$$

$$\frac{\partial^2\mathbf{u}}{\partial p^2}=\left(\mathbf{B}_0-\lambda_0\mathbf{C}_0+\bar{\mathbf{z}}_0\mathbf{z}_0^T\mathbf{C}_0\right)^{-1}\left[\left(2\left(\mathbf{C}_2\lambda_0-\mathbf{B}_2+2\frac{\partial\lambda}{\partial p}\mathbf{C}_1\right)+\mathbf{C}_0\frac{\partial^2\lambda}{\partial p^2}\right)\mathbf{u}_0+2\left(\lambda_1\mathbf{C}_0+\lambda_0\mathbf{C}_1-\mathbf{B}_1\right)\mathbf{u}_1\right]$$

(30)

where

$$\mathbf{u}_1 = \frac{\partial \mathbf{u}}{\partial p}; \quad \mathbf{B}_2 = \frac{1}{2}\frac{\partial^2 \mathbf{B}}{\partial p^2}; \quad \mathbf{C}_2 = \frac{1}{2}\frac{\partial^2 \mathbf{C}}{\partial p^2}. \tag{31}$$

The results in this section are used in the following sections to compute the eigencharacteristics of a system modelled using the WFE approach.

3. The WFE eigenproblem and sensitivity analysis

In this paper the perturbations developed in section 2 are applied to determine the sensitivities of the wavenumbers and wave mode shapes that describe wave propagation in a medium. For simple situations analytical solutions are available, and perturbations follow straightforwardly. The focus here is on more complicated constructions for which the wave characteristics are found using the WFE method.

The WFE method for free wave propagation [2,3] involves developing a finite element model of a short segment of the structure of length Δ as shown in Figure 1. This involves the degrees of freedom (DOFs) $\mathbf{q}$ and nodal forces $\mathbf{f}$ of the segment. The mass and stiffness matrices $\mathbf{M}$ and $\mathbf{K}$ are determined. Time harmonic motion at frequency ω is assumed and the dynamic stiffness matrix (DSM) $\mathbf{D} = \mathbf{K} - \omega^2\mathbf{M}$ is formed. This relates the DOFs and nodal forces by

$$\mathbf{f} = \mathbf{D}\mathbf{q}. \tag{32}$$

Damping can be included by a viscous damping matrix $\mathbf{C}$ or by $\mathbf{K}$ being complex. Under the propagation of a wave, the DOFs and nodal forces at the ends of the segment are related by

$$\mathbf{q}_R = \lambda \mathbf{q}_L; \quad \mathbf{f}_R = -\lambda \mathbf{f}_L; \quad \mathbf{q} = \begin{Bmatrix} \mathbf{q}_L \\ \mathbf{q}_R \end{Bmatrix}; \quad \mathbf{f} = \begin{Bmatrix} \mathbf{f}_L \\ \mathbf{f}_R \end{Bmatrix} \tag{33}$$

where $\lambda = \exp(-ik\Delta)$, with k being the wavenumber, which is generally complex, and the subscripts L, R denote the left and right ends of the segment. The FE model may involve internal nodes and their DOFs condensed. The periodicity conditions in Eq. (33) are applied and an eigenproblem follows, the solutions yielding the eigenvalues $\lambda = \exp(-ik\Delta)$ with the eigenvectors being the wave mode shapes, i.e. the DOFs and nodal forces under the passage of the free wave.

The WFE eigenproblem can be phrased in at least 3 different ways as described below. These result in eigenproblems of the form of Eq. (1). The parameter vector $\mathbf{p}$ may contain any of the material, geometric or physical properties of the segment, or the frequency ω which is involved in the calculation

of the DSM. The results derived in the previous section can then be applied to determine the sensitivity of the eigenvalues and eigenvectors with respect to a parameter.

3.1 The transfer matrix of the segment

The first form of the eigenproblem involves the transfer matrix **T** of the segment. The DSM is partitioned into

$$\mathbf{D}=\begin{bmatrix}\mathbf{D}_{LL} & \mathbf{D}_{LR}\\ \mathbf{D}_{RL} & \mathbf{D}_{RR}\end{bmatrix}, \tag{34}$$

By rearranging Eq. (32), the DOFs **q** and nodal forces **f** at the left and right ends of the segment can be related by

$$\begin{Bmatrix}\mathbf{q}_R\\ \mathbf{f}_R\end{Bmatrix}=\mathbf{T}\begin{Bmatrix}\mathbf{q}_L\\ \mathbf{f}_L\end{Bmatrix};\quad \mathbf{T}=\begin{bmatrix}-\mathbf{E}\mathbf{D}_{LL} & \mathbf{E}\\ -\mathbf{D}_{RL}+\mathbf{D}_{RR}\mathbf{E}\mathbf{D}_{LL} & -\mathbf{D}_{RR}\mathbf{E}\end{bmatrix};\quad \mathbf{E}=\mathbf{D}_{LR}^{-1}, \tag{35}$$

In the notation of Eq. (1), **B** = **T** and **C** = **I**. For the case of a single parameter p the first order matrix derivatives are

$$\mathbf{B}_1=\begin{bmatrix}-\mathbf{E}'\mathbf{D}_{LL}-\mathbf{E}\mathbf{D}_{LL}' & \mathbf{E}'\\ -\mathbf{D}_{RL}'+\mathbf{D}_{RR}'\mathbf{E}\mathbf{D}_{LL}+\mathbf{D}_{RR}\mathbf{E}'\mathbf{D}_{LL}+\mathbf{D}_{RR}\mathbf{E}\mathbf{D}_{LL}' & -\mathbf{D}_{RR}'\mathbf{E}-\mathbf{D}_{RR}\mathbf{E}'\end{bmatrix},\ \mathbf{C}_1=\mathbf{0}, \tag{36}$$

where $\left(\,'\,\right)$ denotes d/dp and $\mathbf{E}'=-\mathbf{E}\mathbf{D}_{LR}'\mathbf{E}$. Given the eigenvalue derivative $\partial\lambda/\partial p$, the derivative of the wavenumber is

$$\frac{\partial k}{\partial p}=\frac{i\exp\left(ik\Delta\right)}{\Delta}\frac{\partial\lambda}{\partial p} \tag{37}$$

While the transfer matrix approach is perhaps the simplest intuitively, it is prone to poor numerical conditioning [18] and this is exacerbated for the case of sensitivity estimation.

3.2 Projection of the equations of motion onto the left-hand DOFs

Projecting the equations of motion onto the left-hand DOFs $\mathbf{q}_L$ leads to a quadratic eigenproblem that can be recast as the linear eigenproblem [2,3]

$$\left[\begin{bmatrix}\mathbf{0} & \mathbf{D}_{RL}\\ -\mathbf{D}_{RL} & -\left(\mathbf{D}_{LL}+\mathbf{D}_{RR}\right)\end{bmatrix}-\lambda\begin{bmatrix}\mathbf{D}_{RL} & \mathbf{0}\\ \mathbf{0} & \mathbf{D}_{LR}\end{bmatrix}\right]\begin{Bmatrix}\mathbf{q}_L\\ \lambda\mathbf{q}_L\end{Bmatrix}=\mathbf{0}. \tag{38}$$

Hence

$$\mathbf{B}=\begin{bmatrix}\mathbf{0} & \mathbf{D}_{RL}\\ -\mathbf{D}_{RL} & -\left(\mathbf{D}_{LL}+\mathbf{D}_{RR}\right)\end{bmatrix},\quad \mathbf{C}=\begin{bmatrix}\mathbf{D}_{RL} & \mathbf{0}\\ \mathbf{0} & \mathbf{D}_{LR}\end{bmatrix} \tag{39}$$

and the matrix derivatives follow straightforwardly.

3.3 The method of Zhong and Williams

Zhong's method [19,20] is the perhaps the most numerically robust approach to solving the eigenproblem, especially for large system matrices. The eigenproblem becomes

$$\left[\mathbf{B}-\mu\mathbf{C}\right]\begin{Bmatrix}\mathbf{q}_L\\ \lambda\mathbf{q}_L\end{Bmatrix},\quad \mathbf{B}=\begin{bmatrix}\mathbf{D}_{RL} & \mathbf{0}\\ \mathbf{0} & \mathbf{D}_{LR}\end{bmatrix},\quad \mathbf{C}=\begin{bmatrix}-\left(\mathbf{D}_{LL}+\mathbf{D}_{RR}\right) & -\left(\mathbf{D}_{LR}-\mathbf{D}_{RL}\right)\\ \left(\mathbf{D}_{LR}-\mathbf{D}_{RL}\right) & -\left(\mathbf{D}_{LL}+\mathbf{D}_{RR}\right)\end{bmatrix}. \tag{40}$$

In this case also the matrix derivatives follow straightforwardly. The double eigenvalues μ in this formulation are related to $\lambda=\exp\left(-ik\Delta\right)$ by

$$\mu=\frac{1}{\left(\lambda+1/\lambda\right)},\quad \lambda=\frac{1\pm\sqrt{1-4\mu^2}}{2\mu} \tag{41}$$

so that the sensitivities are related by

$$\frac{\partial\lambda}{\partial p}=\frac{\left(1+\lambda^2\right)^2}{\left(1-\lambda^2\right)}\frac{\partial\mu}{\partial p} \tag{42}$$

3.4 Group velocity estimation

The group velocity has been estimated in a number of ways using FE-based approaches. For undamped systems it is identical to the energy velocity and can be found by calculating the ratio of the time average energy flow and energy density [2]. Finnveden [21] differentiated the equations of motion of a spectral finite element model, with the resulting solution yielding the group velocity: this is an analogous approach to that developed here for WFE models. Finally, the wavenumbers can be estimated at two, close frequencies and the group velocity estimated by a finite difference approach (e.g. [22]).

In the notation of this paper, the group velocity can be found by choosing the parameter as

$$p = \omega^2 \tag{43}$$

and noting that

$$\frac{\partial \mathbf{D}}{\partial p} = -\mathbf{M} \tag{44}$$

For the second eigenformulation we therefore have

$$\frac{\partial \mathbf{B}}{\partial p} = -\begin{bmatrix} \mathbf{0} & \mathbf{M}_{RL} \\ -\mathbf{M}_{RL} & -(\mathbf{M}_{LL} + \mathbf{M}_{RR}) \end{bmatrix}, \quad \frac{\partial \mathbf{C}}{\partial p} = -\begin{bmatrix} \mathbf{M}_{RL} & \mathbf{0} \\ \mathbf{0} & \mathbf{M}_{LR} \end{bmatrix} \tag{45}$$

with analogous expression for the third eigenformulation. The group velocity for a propagating wave is then given by

$$c_g = \frac{\partial \omega}{\partial k} = \frac{1}{2\omega \partial k / \partial p} \tag{46}$$

and is hence given directly from the calculated wavenumber derivative.

3.5 Estimation of matrix derivatives

The sensitivity analysis requires the matrix derivatives $\partial \mathbf{B}/\partial p$ and $\partial \mathbf{C}/\partial p$. Where analytical expressions for **K** and **M** are available, these derivatives follow immediately. Matrix sensitivities might be available in some commercial and in-house codes, particularly where model updating applications are required. If not, then they can be numerically estimated using a finite difference approximation after generating **K** and **M** for a number of values of the system properties.

4. Numerical examples

In this section various results for the first order sensitivities are presented. For the first example results are compared with analytical predictions. Analytical solutions are not available for the second and third examples.

4.1 Thin beam undergoing axial and bending vibration

Consider a thin beam undergoing axial and bending vibrations. The axial and transverse displacements are *v* and *w* respectively. The axial and bending wavenumbers of the propagating waves are respectively [23]

$$k_a = \omega\sqrt{\frac{\rho}{E}}; \quad k_b = \sqrt[4]{\frac{\rho A\omega^2}{EI}} \tag{47}$$

where E, ρ, A and I are respectively the elastic modulus, density, cross-sectional area and second moment of area. There is also a bending nearfield wave, which decays exponentially with distance, and is not considered further. The group velocities are

$$c_{g,a} = \sqrt{\frac{E}{\rho}}; \quad c_{g,b} = \frac{1}{2}\sqrt[4]{\frac{EI\omega^2}{\rho A}} \tag{48}$$

The WFE model consists of a single, two-noded element with 3 nodal DOFs $\mathbf{q} = \left[v, w, \partial w/\partial x\right]^T$ at each node. The shape functions for axial and transverse displacements are taken as linear and cubic functions of x respectively, leading to the mass and stiffness matrices given in Appendix A [24].

Figure 2 shows the wavenumbers, taking $E = 210\times10^9$ N/ m^2, $\rho = 7850$ kg/m^3, thickness = 15 mm and width = 30 mm. At the largest frequency shown $k\Delta \approx 1$ and hence FE discretisation errors are noticeable. The numerical predictions are almost real-valued, with the imaginary parts (not shown) resulting from rounding errors etc. The projection method (section 3.2) and Zhong's method (section 3.3) give virtually identical results, with results using the projection method shown. The agreement with the theory is very good but of decreasing accuracy as frequency increases due to discretisation effects. The transfer matrix approach, however, suffers from poor numerical conditioning and yields accurate solutions only up to a frequency of approximately $\omega = 4\times10^4$ rad/s and results are not shown.

The analytical sensitivities of the wavenumbers with respect to the material parameters are

$$\frac{\partial k_a}{\partial \rho} = \frac{\omega}{2\sqrt{\rho E}}, \quad \frac{\partial k_a}{\partial E} = -\frac{\omega}{2E}\sqrt{\frac{\rho}{E}} \tag{49}$$

$$\frac{\partial k_b}{\partial \rho} = \frac{\omega^{1/2}}{4\rho}\left(\frac{A\rho}{EI}\right)^{1/4}, \quad \frac{\partial k_b}{\partial E} = -\frac{\omega^{1/2}}{4E}\left(\frac{A\rho}{EI}\right)^{1/4}. \tag{50}$$

The sensitivities, evaluated using the method described in section 3.2, are shown in Figure 3, while Figure 4 shows the analytical and predicted group velocities. Figure 5 shows the absolute values of the relative errors for wavenumber, sensitivities and group velocity. The agreement is good, with relative errors increasing as frequency increases, typically as ω^2. Given that at the highest frequency shown $k_b\Delta \approx 1$, FE discretisation effects would be expected to be apparent. For this example, the numerical

results for the sensitivities and group velocity are virtually identical. Note that the sensitivities and group velocity are up to an order of magnitude less accurate than wavenumber estimates, while the accuracy of the results for the axial waves is up to an order of magnitude worse for axial waves than bending waves, due in part to the fact that a higher order FE shape function is used to describe the bending behaviour.

4.2 Foam cored panel

The second example is the sandwich panel shown in Figure 6. The skins are 0.5mm thick ($E = 4.9\times10^{10}\,\text{Pa},\ \rho = 1600\text{kg/m}^3$ and Poisson's ratio $\nu = 0.15$) while the core is 6.35mm thick foam ($E = 8.3\times10^{9}\,\text{Pa},\ \rho = 160\text{kg/m}^3$ and $\nu = 0.34$). Damping is neglected here to ensure that the propagating wavenumbers are real, but it is straightforward to include a complex elastic modulus, especially for the core. All wavenumbers are then complex. Figure 6 also indicates the FE mesh of the cross-section that was used. One ANSYS SOLID 45 element (now implemented within SOLID 185) was used to mesh each skin and 6 elements used to mesh the core, giving a total of 8 elements. Each element has 8 nodes, each of which has three nodal degrees of freedom, in-plane and transverse displacements, giving 27 DOFs in the WFE model. The length of the meshed region was Δ=0.001m, which gives good accuracy for wavenumbers up to about k=1000/m.

The wavenumbers for this isotropic structure are shown in Figure 7(a). In the frequency range shown there are three propagating waves, these broadly being extensional, shear and bending waves of the plate. Further propagating waves cut off at higher frequencies and involve higher order modes across the thickness of the sandwich panel. Figure 7(b) shows the normalised sensitivities $\left(G/k\right)dk/dG$ of the wavenumbers with respect to the shear modulus of the core. The matrix derivatives were estimated using a finite difference approximation, varying G by ±10%. As would be expected, the axial wavenumber is insensitive to the shear modulus, while the shear wavenumber is very sensitive, while the bending wave is increasingly sensitive to the shear modulus of the core as frequency increases.

4.3 Cross-laminated timber panel

Cross-laminated timber (CLT) panels are constructed from a number of layers of wooden beams laid at right-angles in adjacent layers and bonded with adhesive [25] (Figure 8). Layering the timber in this way gives a relatively high stiffness in all directions for the wooden panel, which has relatively low mass compared with other traditional building materials such as concrete or brick [26]. Because of these advantages, and the fact that CLT structures can be assembled quickly and easily on-site, CLT is gaining in popularity as a building material in many countries [27]. However, due to their low mass and high stiffness, CLT structures are prone to poor acoustic performance, both for sound transmission over the whole audio-frequency range and for structure-borne sound transmission, typically impact noise below

1kHz. The vibroacoustic behaviour is not well understood and is a subject of current research activity, given that there is a need for improved design tools.

The properties of wood are highly uncertain and depend on many factors including the tree growing conditions, what part of the tree the wood is taken from, the direction in which the panel is cut, knots, grain slope etc. The elastic properties along- and cross-grain differ by an order of magnitude [28]. For example, the density of radiata pine varies from 340-540 kg/m^3 while the along-grain elastic modulus ranges from 6-14 GPa, correlates to some degree with density and is substantially higher than the cross-grain value [29]. The mechanical properties of a specific panel often need to be determined from experimental measurements, while uncertainty modelling is required to develop robust designs.

The CLT panel considered here has 6 layers of equal thickness and is 0.1m thick in total. The nominal properties are listed in Table 1. The segment in the WFE model is 5mm square, with 3 ANSYS SOLID 45 elements per layer, giving 18 elements in total and 57 DOFs at each corner of the segment. This structure is anisotropic, so that the wavenumbers depend on the direction of wave propagation. Numerical results for waves propagating in the global *y*-direction are presented, with the wavenumber in the other in-plane direction being set to zero.

The propagating wavenumbers are shown in Figure 9. At low frequencies (Figure 9(a)) there are 3 propagating wave modes dominated by bending, in-plane shear and in-plane axial motion. As frequency increases, the "bending" mode becomes increasingly affected by shear in the transverse layers. At higher frequencies many other wave modes cut on, involving through-thickness effects, including substantial shear in the weaker layers, significant symmetric transverse displacements etc. The wave characteristics are considered in detail in [30]. The sensitivity with respect to the along-grain elastic modulus dk/dE_x and the normalised sensitivity $\left(E_x/k\right)dk/dE_x$ are shown in Figures 10 and 11. At lower frequencies (Figure 10), where the behaviour can be interpreted as an equivalent plate, the axial and bending wave modes are seen to be sensitive to E_x while the shear wave mode is insensitive, as would be expected. The axial wave has a normalised sensitivity of approximately -0.5, the same as axial waves in a homogeneous solid, the cross-grain stiffness of the transverse layers being very small. The normalised sensitivity of the bending wave tends to -0.25 at zero frequency, the same value as the bending wave in a homogeneous thin plate, but the effects of shear in the transverse layers become significant at low frequencies, the dependence of the sensitivity with frequency changing from $\omega^{1/2}$ to approximately ω^1. At higher frequencies (Figure 11) the behaviour is very complicated. Higher wave modes cut on above 1kHz, involving through-thickness effects where the motion can no longer be regarding as that of an equivalent plate. These modes can be important both for sound transmission and structure-borne sound [30]. Note that around 2300 Hz two wave modes appear to lock and veer (see

Figure 9(b)), with the sensitivities in Figure 11 becoming very large: here, two eigenvalues become equal so that the eigenvalue sensitivities developed in section 2 are no longer valid.

5. Concluding remarks

In this paper a perturbation approach was used to evaluate the first order and second order sensitivities of the eigenproperties of complex, non-symmetric matrices. The results were then applied to wave and finite element models to estimate the sensitivity of the wavenumber with respect to system parameters. Expressions for the group velocity were derived. Three different eigenformulations were presented, namely, the transfer matrix method, the projection method and Zhong's method. Numerical results for a thin beam, a foam cored panel and a cross-laminated timber panel were presented to demonstrate the applicability of the proposed approach. The computational cost over and above the generation of the FE matrices is small: for example, for the last, most complicated, example, wavenumbers, wave mode shapes and sensitivities were calculated using non-optimised Matlab code at less than 10ms per frequency.

It is worth noting that the sensitivity expressions derived break down for the case of equal (or very close) eigenvalues. There are two situations, termed weak or strong interaction in [5], corresponding to mode crossing or veering/instability in modal analysis, or wavenumber crossing or veering/locking for wave propagation. For spatially varying properties, additional problems arise at and around any critical sections, also known as turning points, at which part of a waveguide of a particular wave mode is propagating in one frequency range (cut-on transition), while it is non-propagating in another range (cut-off transition). As a result, the changes in the characteristics of wave propagation at these critical sections typically lead to strong wave reflections. These situations are the subject of future work.

There are various potential applications of the results developed here. The first is the calculation of group velocity (section 3.4) for which the matrix derivatives just depend on the mass matrix (equation (45)). Note also that the group velocity is calculated independently for each branch of the dispersion curve, in contrast to finite difference approaches, where the dispersion curves have to be tracked from one frequency to the next: this is problematical where two branches are close and may cross, veer or lock. A second area of application concerns uncertainty modelling, and the propagation of uncertainties in properties to uncertainties in various response quantities: for example, on-going work includes the effects of material variability in CLT panels on the air- and structure-borne noise performance, which depend on wavenumbers etc, and the attempt to put bounds on the performance. A third area concerns model updating, for example using measured wavenumbers to update a WFE model.

Acknowledgements

The authors gratefully acknowledge the support of the Royal Society for support under the International Exchanges programme IES\R3\170279 and the MBIE Smart Ideas grant entitled “A Wave and Finite Element Method for Calculating Sound Transmission in Lightweight Buildings”.

References

[1] L. Cremer, M. Heckl and B.A.T. Petersson, Structure-Borne Sound (3rd Edition), Springer-Verlag, 2005.

[2] B. R. Mace, D. Duhamel, M. J. Brennan, L. Hinke, Finite element prediction of wave motion in structural waveguides. Journal of the Acoustical Society of America, 117, 2835-2843, 2005.

[3] D. Duhamel, B. R. Mace, M. J. Brennan, Finite element analysis of the vibration of waveguides and periodic structures. Journal of Sound and Vibration, 294, 205-220, 2006.

[4] R. L. Fox and M.P. Kapoor, Rate of change of eigenvalues and eigenvectors, AIAA J, 6 (12), 2426-2429, 1968.

[5] Seyranian A.P.; Mailybaev A.A.: Multiparameter Stability Theory with Mechanical Applications, World Scientific Publishing, Singapore, 2003.

[6] A.P. Seyranian, Sensitivity analysis of multiple eigenvalues. J Str Mech, 21, 261-284, 1993.

[7] A.P. Seyranian, A.A. Mailybaev, Interaction of eigenvalues in multi-parameter problems, Journal of Sound and Vibration, 267 (5), 1047-1064, 2003.

[8] Y. Yang, B. R. Mace, M. J. Kingan, Prediction of sound transmission through, and radiation from, panels using a wave and finite element method, The Journal of the Acoustical Society of America 141 (4), 2452-2460, 2017.

[9] Y. Yang, B. R. Mace, M. J. Kingan, A wave and finite element based homogenised model for predicting sound transmission through honeycomb panels, Journal of Sound and Vibration 463, 114963. 2019.

[10] Y. Yang, B. R. Mace, M. J. Kingan, Vibroacoustic analysis of periodic structures using a wave and finite element method, Journal of Sound and Vibration 457, 333-353, 2019.

[11] B. E. Takiuti, E. Manconi, M.J. Brennan, V. Lopes Junior, Wave transmission from asymmetrical changes of cross-sectional area in a beam, Journal of Physics: Conference Series, Volume 1264, Thirteenth International Conference on Recent Advances in Structural Dynamics (RASD) 15–17 April 2019, Valpre, Lyon, France.

[12] G. Mitrou, N. Ferguson, J. Renno, Wave transmission through two-dimensional structures by the hybrid FE/WFE approach, . Journal of Sound and Vibration. 389, 484-501, 2017.

[13] F. Errico, F .Franco, M. Ichchou, An investigation on the vibrations of laminated shells under aeroacoustic loads using a WFE approach, Advances in Aircraft and Spacecraft Science, 6(6), 463-478, 2019.

[14] E. Manconi, S. Sorokin, R. Garziera, A. Soe-Knudsen, Wave motion and stop-bands in pipes with helical characteristics using wave finite element analysis, Journal of Applied and Computational Mechanics, 4(5):420-428, 2018.

[15] F. Errico, M. Ichchou, S. De Rosa, O. Bareille, F. Franco, A WFE and hybrid FE/WFE technique for the forced response of stiffened cylinders, Advances in Aircraft and Spacecraft Science , 5(1), 1-19, 2018.

[16] Cha P.D., Shin A., Perturbation methods for the eigencharacteristics of the symmetric and asymmetric systems, Shock and Vibration, 2018.

[17] V. A. Yakubovich, V. M. Starzhinskii, Parametric resonance in linear systems, Nauka, Moscow (in Russian), 1987.

[18] Y. Waki, B.R. Mace and M.J. Brennan, Numerical issues concerning the wave and finite element method for free and forced vibrations of waveguides. Journal of Sound and Vibration, 327, 92-108, 2009.

[19] W.X. Zhong, F.W. Williams, On the direct solution of wave propagation for repetitive structures, Journal of Sound and Vibration 181 (1995) 485–501.

[20] W. X. Zhong, F. W. Williams Wave Problems for Repetitive Structures and Symplectic Mathematics, Proc Institution of Mechanical Engineers, Part C 206, 371-379, 1992.

[21] S. Finnveden, "Evaluation of modal density and group velocity by a finite element method," J. Sound Vib. 273, 51-75 (2004).

[22] M.N.Ichchou, S.Akrout and J.-M.Mencik. "Guided waves group and energy velocities via finite elements," J Sound Vib 305, 931-944 (2007)

[23] K. F. Graff, Wave Motion in Elastic Solids, Dover Publications Inc., New York, 1975.

[24] M. Petyt, *Introduction to finite element vibration analysis*, Cambridge University Press, New York, USA (1990).

[25] Z. Wang, J. Zhou, W. Dong, Y. Yao, M. Gong, Influence of technical characteristics on the rolling shear properties of cross laminated timber by modified planar shear tests, Maderas. Ciencia y tecnología, 20 (2018) 469-478.

[26] F. Morandi, S. De Cesaris, M. Garai, L. Barbaresi, Measurement of flanking transmission for the characterisation and classification of cross laminated timber junctions, Applied Acoustics, 141 (2018) 213-222.

[27] R. Brandner, G. Flatscher, A. Ringhofer, G. Schickhofer, A. Thiel, Cross laminated timber (CLT): overview and development, European Journal of Wood and Wood Products, 74 (2016) 331-351.

[28] J.A. Kininmonth, L. Whitehouse, Properties and uses of New Zealand radiata pine, (1991).

[29] A. Homb, C. Guigou-Carter, A. Rabold, Impact sound insulation of cross-laminated timber/massive wood floor constructions: Collection of laboratory measurements and result evaluation, Building Acoustics, 24 (2017) 35-52.

[30] Y. Yang, M. J. Kingan and B. R. Mace, "Analaysis of the acoustic characteristics of cross-laminated timber panels using a wave and finite element method." Proc ICSV 26, Montreal (2019).

Appendix A Mass and stiffness matrices for thin beam

For axial vibrations, the nodal DOF vector is $\mathbf{q} = \begin{bmatrix} v_L & v_R \end{bmatrix}^T$ and the element matrices for an element of length L are [16]

$$\mathbf{M}_a = \frac{\rho AL}{6}\begin{bmatrix} 2 & 1 \\ 1 & 2 \end{bmatrix}; \quad \mathbf{K}_a = \frac{EA}{L}\begin{bmatrix} 1 & -1 \\ -1 & 1 \end{bmatrix} \tag{51}$$

For bending vibrations, the nodal DOF vector is $\mathbf{q} = \begin{bmatrix} w_L & \partial w_L/\partial x & w_R & \partial w_R/\partial x \end{bmatrix}^T$ and the element matrices are [16]

$$\mathbf{M}_b = \frac{\rho AL}{420}\begin{bmatrix} 156 & 22L & 54 & -13L \\ & 4L^2 & 13L & -3L^2 \\ & & 156 & -22L \\ SYM & & & 4L^2 \end{bmatrix}; \quad \mathbf{K}_b = \frac{EI}{L^3}\begin{bmatrix} 12 & 6L & -12 & 6L \\ & 4L^2 & -6L & 2L^2 \\ & & 12 & -6L \\ SYM & & & 4L^2 \end{bmatrix} \tag{52}$$

For an element undergoing both axial and bending vibrations, the nodal DOF vector is $\mathbf{q} = \begin{bmatrix} v_L & w_L & \partial w_L/\partial x & v_R & w_R & \partial w_R/\partial x \end{bmatrix}^T$ and the mass and stiffness matrices follow by assembling the matrices above. Note that derivatives with respect to the material properties E and ρ and the geometric properties A and I follow straightforwardly.

Table 1. Material properties and stacking sequence of CLT panel. The local *x*-axis of each layer is along the grain and aligned at the angle relative to the global *x*-axis specified in the stacking sequence row.

Material property	
$E_x \left[\mathrm{N.m^{-2}}\right]$	1.1×10^{10}
$E_y \left[\mathrm{N.m^{-2}}\right]$	3.67×10^{8}
$E_z \left[\mathrm{N.m^{-2}}\right]$	3.67×10^{8}
$G_{xy} \left[\mathrm{N.m^{-2}}\right]$	6.9×10^{8}
$G_{yz} \left[\mathrm{N.m^{-2}}\right]$	6.9×10^{7}
$G_{xz} \left[\mathrm{N.m^{-2}}\right]$	6.9×10^{8}
ν_{xy}	0.42
ν_{yz}	0.3
ν_{xz}	0.42
η	0.02
$\rho \left[\mathrm{kg.m^{-3}}\right]$	450
Stacking sequence	0° / 90° / 0° / 0° / 90° / 0°

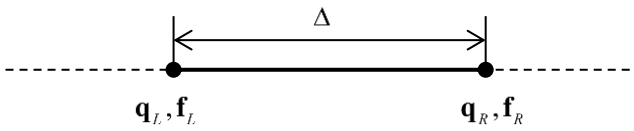

Figure 1. A segment of a uniform waveguide.

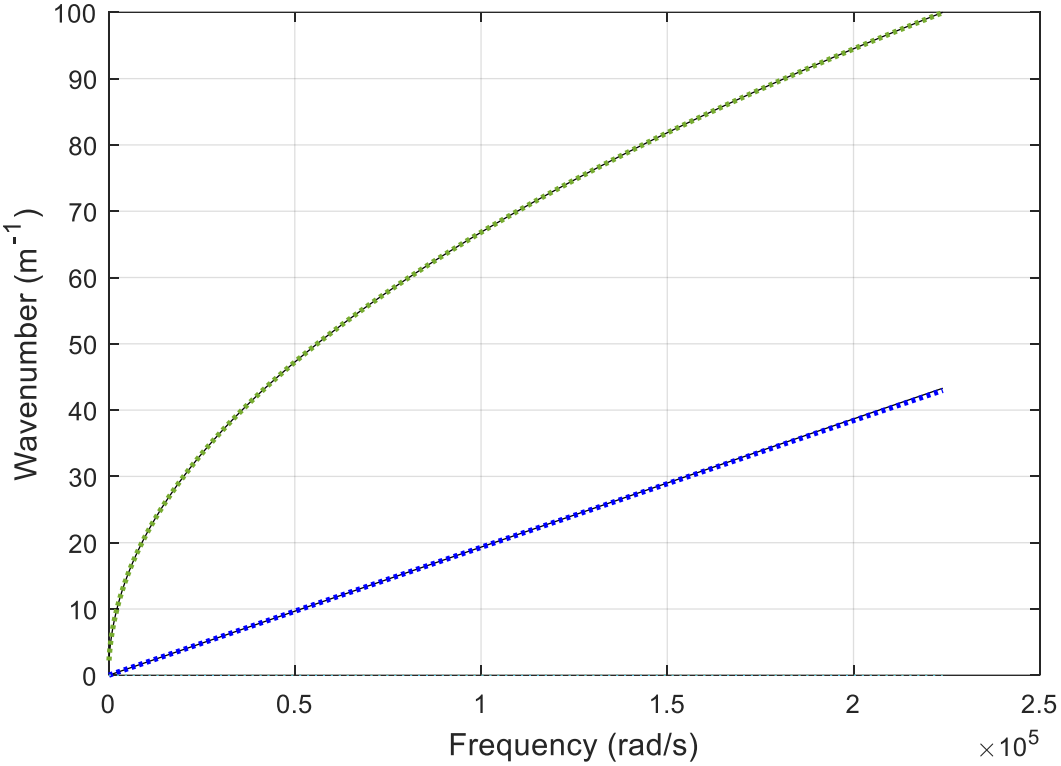

Figure 2. Wavenumbers for a beam: bending and axial waves; theory (solid line) and WFE predictions (dotted line).

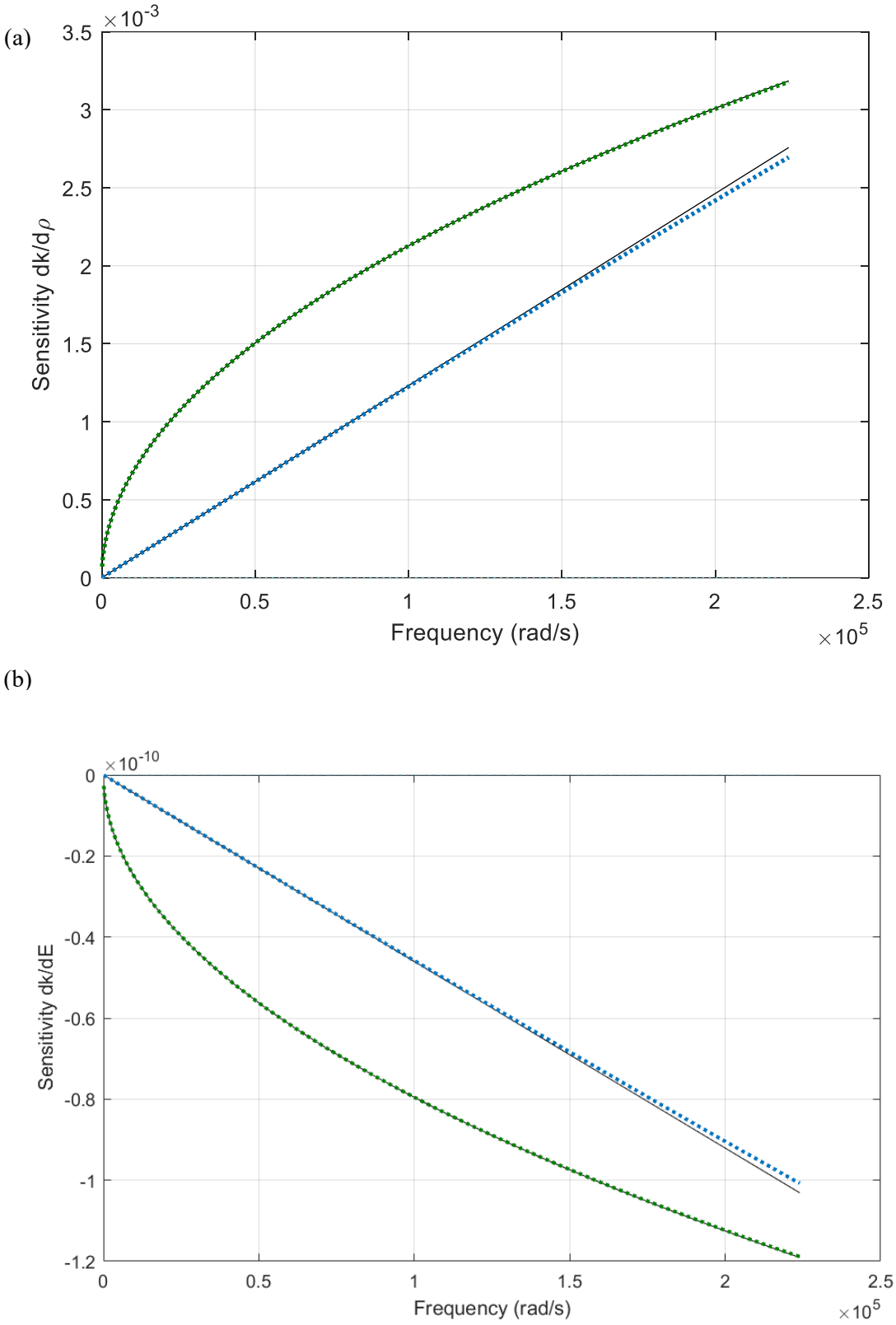

Figure 3. Wavenumbers for a beam: bending and axial waves; (a) sensitivity with respect to density ρ, (b) sensitivity with respect to elastic modulus E; theory (solid line) and WFE predictions (dotted line).

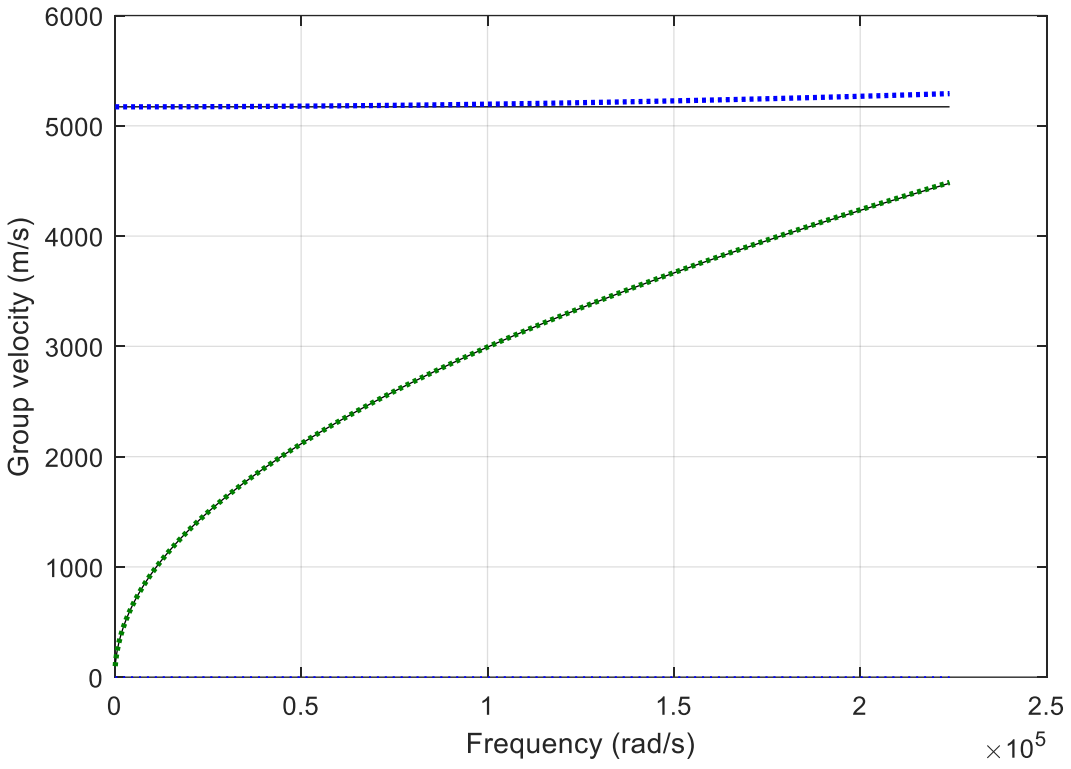

Figure 4. Group velocity for a beam: bending and axial waves; theory (solid line) and WFE predictions (dotted line).

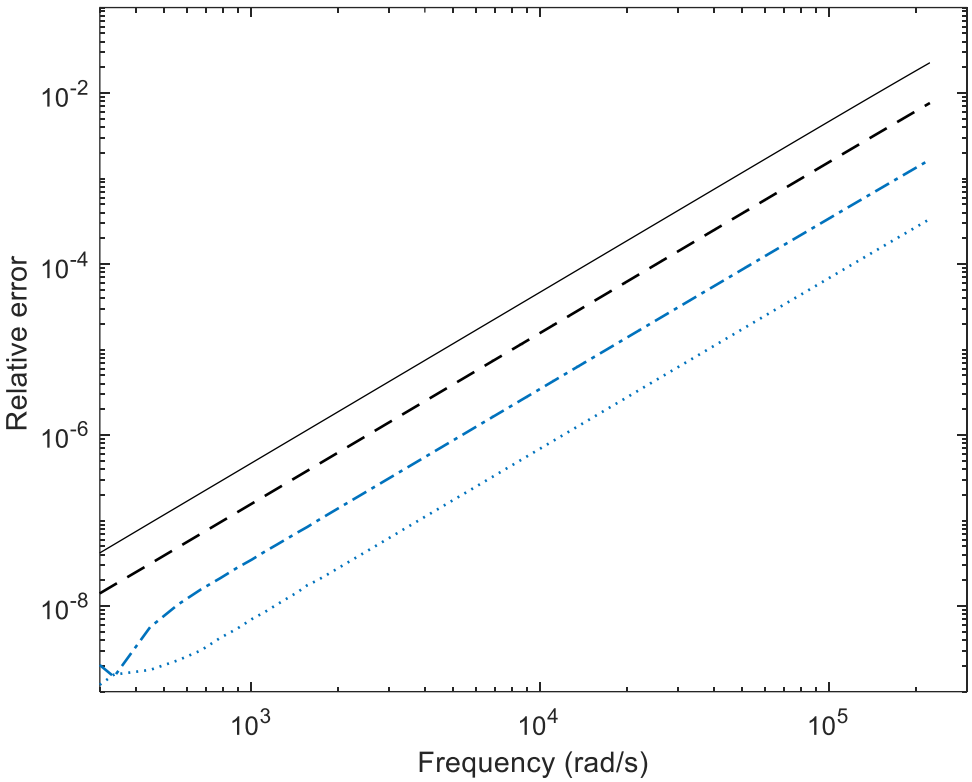

Figure 5. Relative errors for a beam: wavenumbers and group velocity for bending (dotted) and axial (dashed) waves; sensitivity with respect to r or E for bending (dash-dor) and axial (solid) waves.

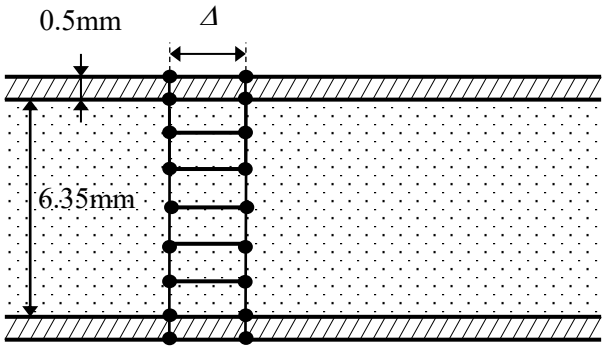

Figure 6. Foam-cored sandwich panel and FE mesh.

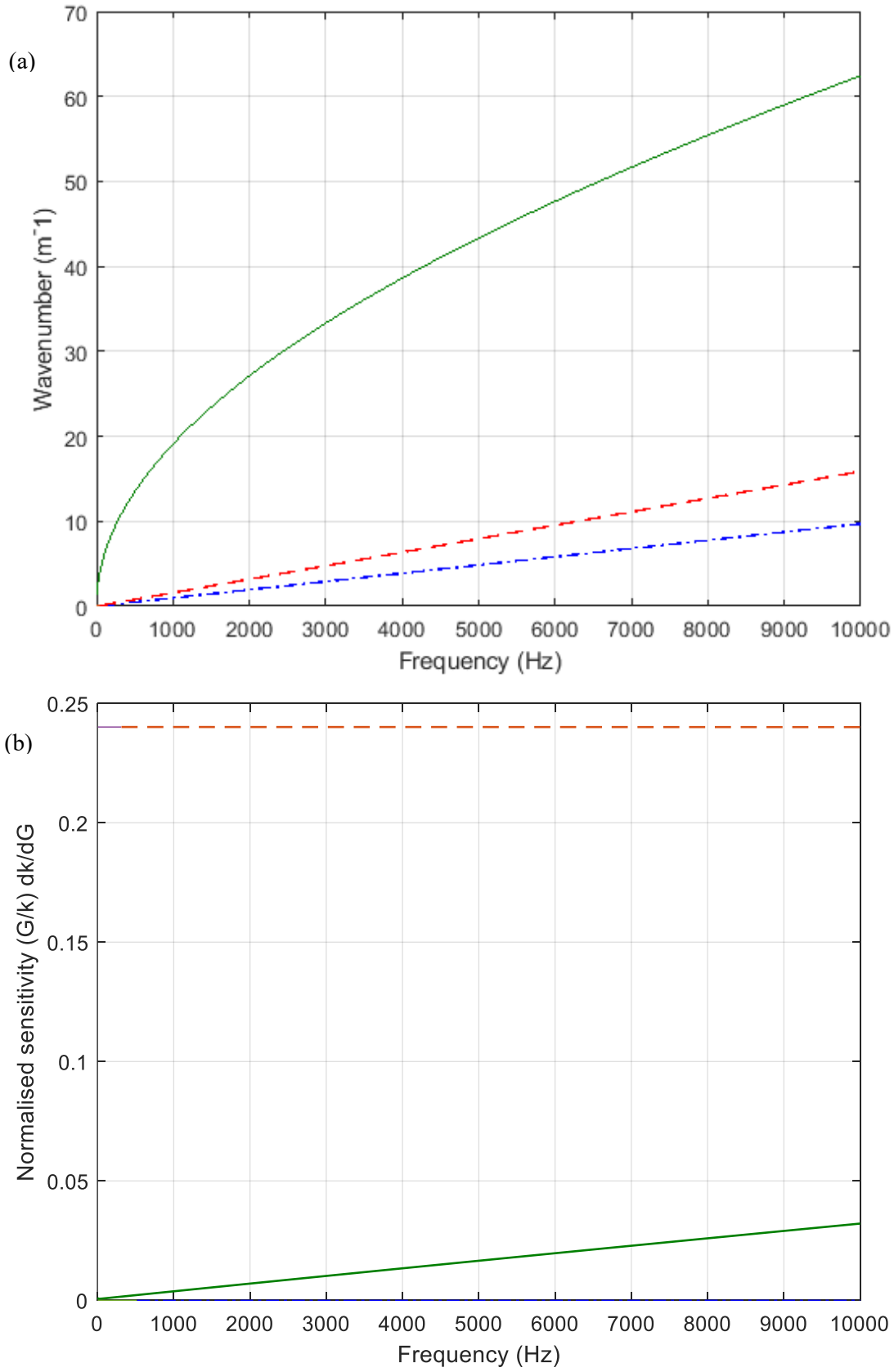

Figure 7. Foam-cored panel: (a) wavenumbers and (b) normalised sensitivity of wavenumbers with respect to shear modulus of the core: bending, shear and axial dominated waves.

Figure 8. Cross-laminated timber panel.

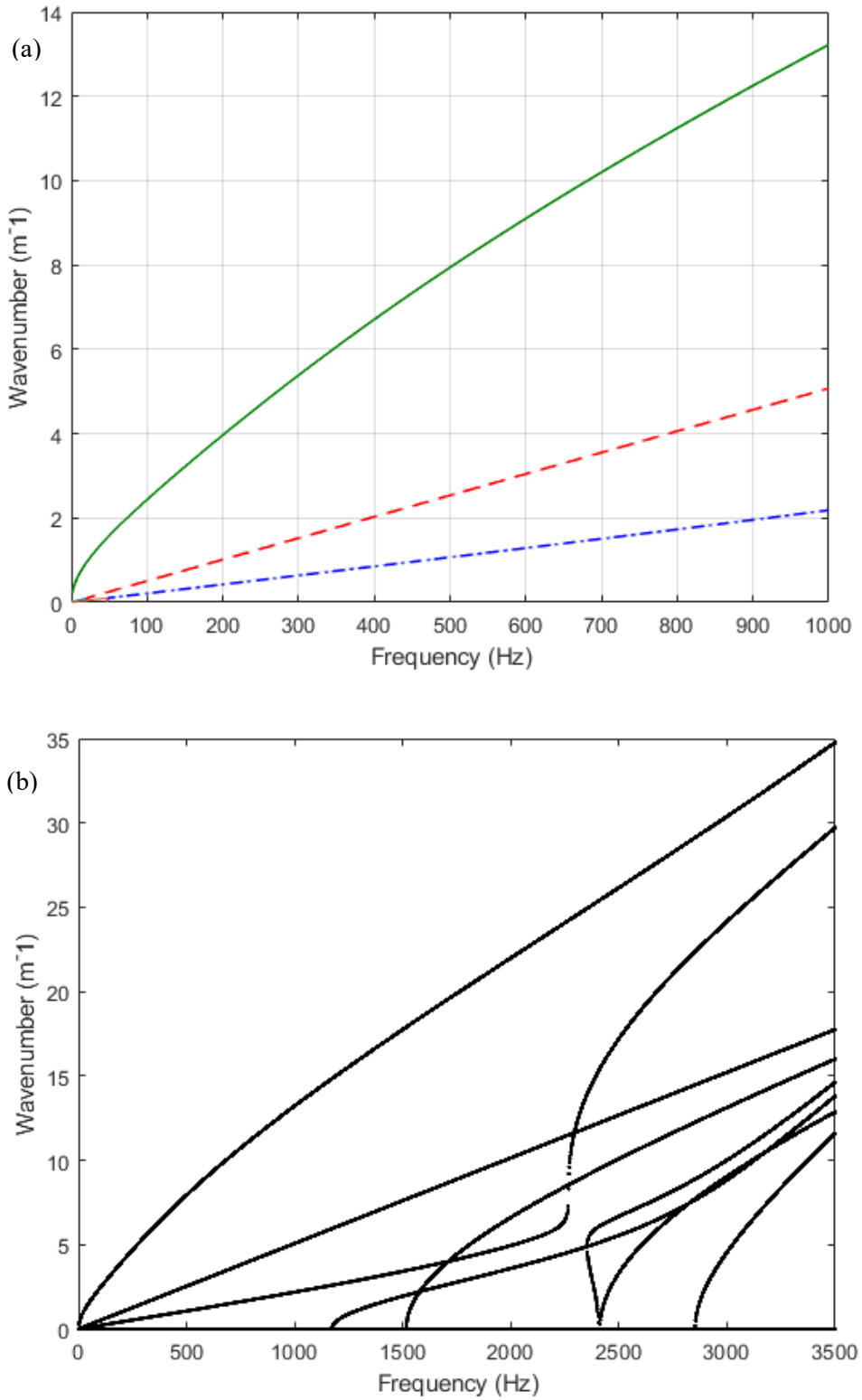

Figure 9. Wavenumbers for CLT panel: (a) lower frequencies bending, shear and axial dominated waves. and (b) higher frequencies:

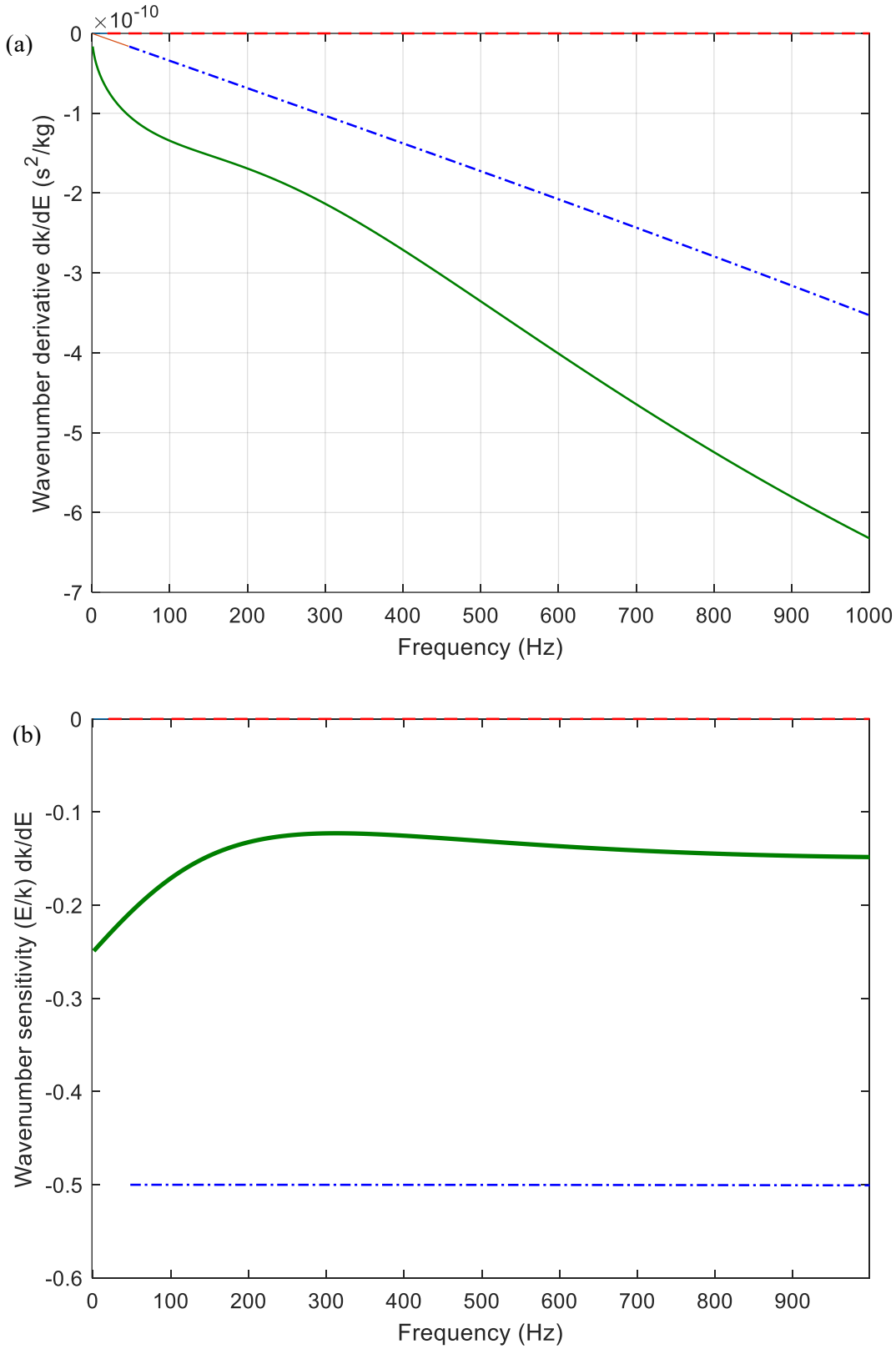

Figure 10. CLT panel: (a) sensitivity and (b) normalised sensitivity of wavenumbers with respect to elastic modulus along-grain, lower frequencies: bending, shear and axial dominated waves.

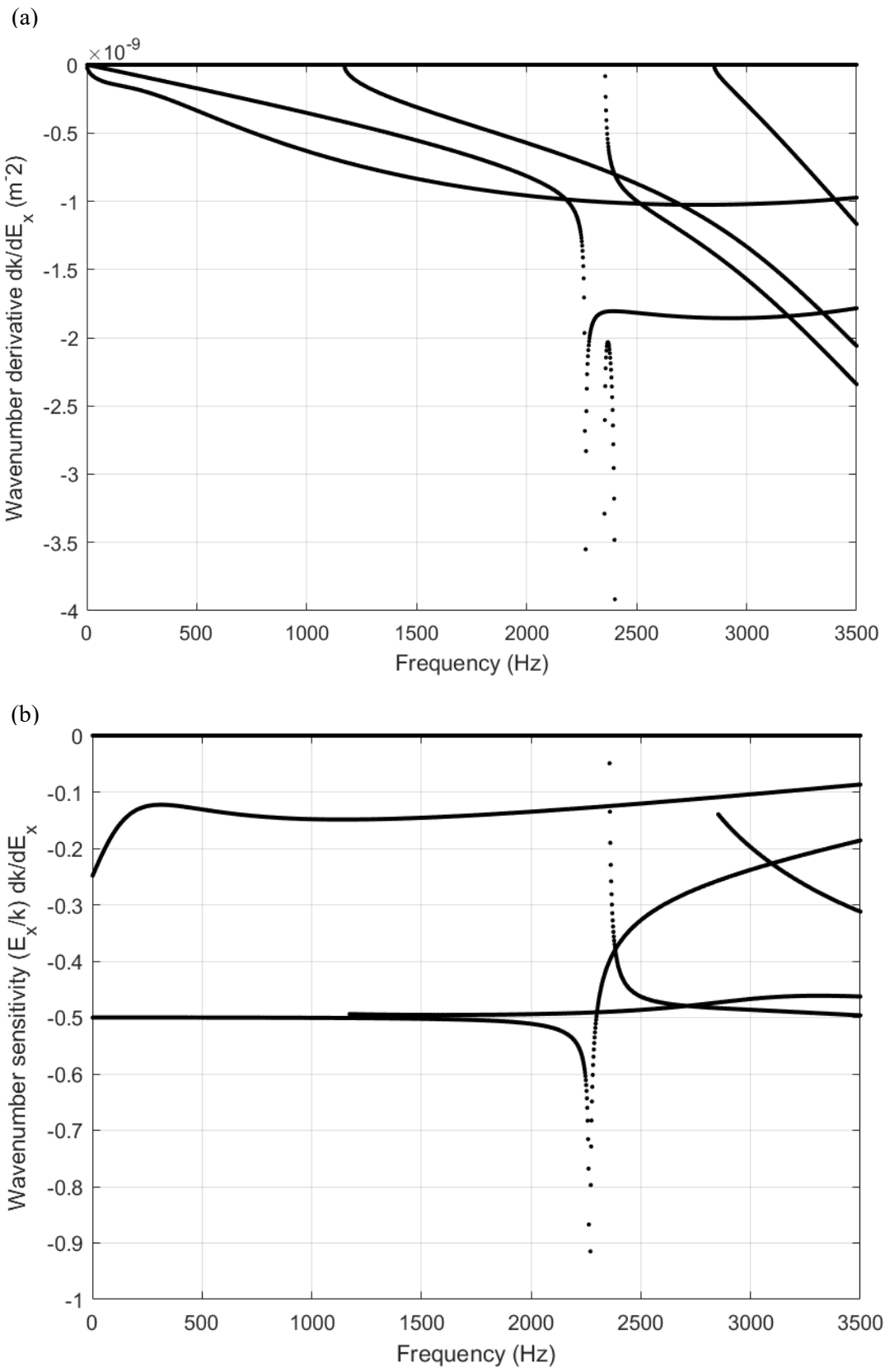

Figure 11. CLT panel: (a) sensitivity and (b) normalised sensitivity of wavenumbers with respect to elastic modulus along-grain, higher frequencies.